Fluid simulations of frequency effects on nonlinear harmonics in inductively coupled plasma

Xue-Jiao Si,[1] Shu-Xia Zhao,[1,2] Xiang Xu,[1] A. Bogaerts,[2] and You-Nian Wang[1,a)]
[1]*School of Physics and Optoelectronic Technology, Dalian University of Technology, Dalian 116024, China*
[2]*Department of Chemistry, University of Antwerp, Campus Drie Eiken, Universiteitsplein 1, BE-2610 Wilrijk-Antwerp, Belgium*

(Received 28 January 2011; accepted 14 February 2011; published online 16 March 2011)

A fluid model is self-consistently established to investigate the harmonic effects in an inductively coupled plasma, where the electromagnetic field is solved by the finite difference time domain technique. The spatiotemporal distribution of harmonic current density, harmonic potential, and other plasma quantities, such as radio frequency power deposition, plasma density, and electron temperature, have been investigated. Distinct differences in current density have been observed when calculated with and without Lorentz force, which indicates that the nonlinear Lorentz force plays an important role in the harmonic effects, especially at low frequencies. Moreover, the even harmonics are larger than the odd harmonics both in the current density and the potential. Finally, the dependence of various plasma quantities with and without the Lorentz force on various driving frequencies is also examined. It is shown that the deposited power density decreases and the depth of penetration increases slightly because of the Lorentz force. The electron density increases distinctly while the electron temperature remains almost the same when the Lorentz force is taken into account. © *2011 American Institute of Physics*. [doi:10.1063/1.3566007]

I. INTRODUCTION

Inductively coupled plasmas (ICPs) have been widely used in the semiconductor manufacturing industry,[1] e.g., for wafer etching,[2,3] thin-film deposition,[4] and nanoscale synthesis and processing.[5] Numerous theoretical and experimental activities have focused on various phenomena in radio frequency (rf) ICPs, especially driven by rf powers with a frequency of 13.56 MHz.[6–9] However, low frequency and low pressure inductive sources are attracting special interest due to their many advantages, such as high transfer efficiency[10] and highly uniform and high-density plasma in large volumes.[11,12] Moreover, many interesting physical phenomena will occur in ICPs operating at low pressure and frequency, such as the anomalous skin effect,[13–15] nonlocal heating,[16,17] and E-H mode transition,[18–20] which are known as the nonlinear effects.

Among these nonlinear mechanisms, harmonic effects in particular have received attention in the past ten years. The harmonic effects, which are induced by the nonlinear Lorentz force localized within the skin layer, can affect the electron dynamics and the plasma quantities, especially at low driving frequency. The axial and radial second harmonic current densities, which are more obvious at low driving frequency, have been observed experimentally with Langmuir probes.[21] This trend was ascribed to the nonlinear Lorentz force, which was characterized as the interaction between the electron azimuthal velocity and the magnetic field.

Based on a slab coordinate system, Cohen *et al.*[22] have derived the reduced orbit equations and obtained the general expressions for the energy gain and density reduction by including the effect of an electrostatic potential. Using this method, they predicted the second harmonic electrostatic potential in the skin region. The harmonic generation of the rf plasma potential has also been measured with a rf probe.[23–25] The experimental results showed that all even harmonics were higher than the odd ones next to it and the second one will be the largest. This phenomenon was attributed to the nonlinear effect caused by the Lorentz force due to the rf magnetic field in the skin layer. Moreover, the relative level of all even harmonics will increase with discharge power.[24] The mechanisms for the generation of nonlinear currents and nonlinear polarization fields in ICP have been analytically investigated, concentrating on the modification of Ohm's law by the Lorentz force and nonlinear inertia.[26]

The expressions for the nonlinear second harmonic and ponderomotive forces in an inhomogeneous rf field have been derived from the electron equation of motion.[27] It was shown that in a collisionless plasma, the second harmonic force and the ponderomotive force are similar in magnitude and frequency dependence. However, both forces became lower and showed a different frequency dependence in a collisional plasma. The second harmonic nonlinear azimuthal magnetic field in electromagnetic (H) mode, measured by miniature magnetic probes, was larger than the fundamental frequency component in H mode.[28] Moreover, a plasma model was established in Ref. 28 to explain the generation of the second harmonics of the azimuthal magnetic field. This effect was attributed to the interactions of the fundamental frequency components of radial and axial magnetic fields with the azimuthal rf current.

The harmonic content of the electron energy distribution function (EEDF) using the "on-the-fly" Monte Carlo method has indicated that the second harmonic dominated the time dynamics of the EEDF and the harmonic component was

a)Electronic mail: ynwang@dlut.edu.cn.

higher at higher energies, as reported by Kushner and co-workers.[29]

Smolyakov *et al.*[30] have summarized the nonlinear effects in inductive discharges, including nonlinear polarization field, electric current, and ponderomotive force. Moreover, they analyzed the structure of the nonlinear forces which contained two parts, the potential part which leads to plasma polarization and the solenoidal part which is responsible for generation of the nonlinear electric current.

However, most work about the harmonic effects was experimentally performed. In the limited theoretical research, the assumption of the spatial variation of both n_e and T_e (Ref. 28) and the single electron approach in the local approximation,[26] as well as the thermal effects,[27] were always neglected in the models. To the authors' knowledge, a self-consistent computer simulation about the harmonic effects has not yet been reported. Besides, the harmonic approximation was assumed in the Maxwell equations, which means that the plasma current also changes as the harmonic form. However, nonlinear plasma polarization will appear because of the wave propagation in plasma, especially at low driving frequency. Thus, we can expect that the harmonic approximation will no longer be suitable since obvious nonlinear effects will occur at low frequency. Therefore, in this paper, we have developed a two-dimensional self-consistent fluid model, including the full set of Maxwell equations to describe the behavior of the harmonic effects. The study is important because the nonlinear plasma polarization will affect the behavior of the current density and potential. Furthermore, the current density and potential will influence the plasma quantities, such as the deposited power density, plasma density, electron temperature, and azimuthal electric field, as well as the plasma uniformity. The aim of our paper is to elucidate the important role of the nonlinear Lorentz force in harmonic effects.

This paper is organized as follows: In Sec. II, the theoretical model including the electromagnetic model and fluid model is described, together with the boundary conditions and the solving technique for these equations. Comparison of harmonic currents with and without Lorentz force and differences among the harmonic current density, the potential, and the evolution of plasma parameters at different frequencies are presented in Sec. III. Finally, conclusions are given in Sec. IV.

II. THEORETICAL MODEL

The simulations are performed for a planar ICP source, which is shown in Fig. 1. It includes three regions: the vacuum vessel region ($h_2 < z < h_3$), the dielectric window region ($h_1 < z < h_2$), and the plasma region ($0 < z < h_1$). Four-turn coils are located on the bottom of the vacuum vessel ($z = h_2$) to excite and maintain the plasma, at $r = 2$, 4, 6, and 8 cm, respectively. The antenna, driven by a generator producing a sine wave coil current, is separated from the plasma by a dielectric window. The current in the coil produces a time-varying magnetic field, which will induce an azimuthal electric field in the plasma region.

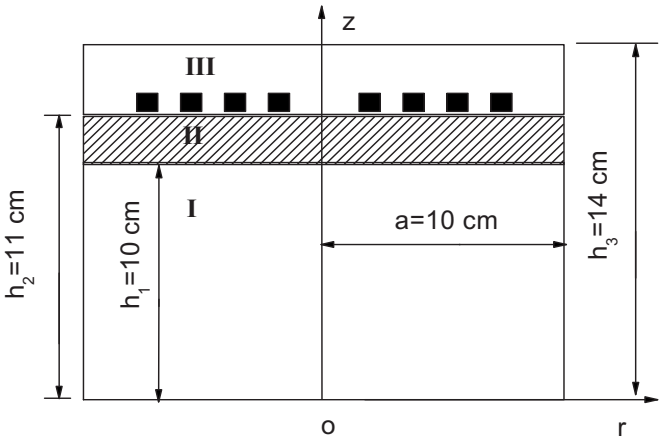

FIG. 1. Schematic picture of the cylindrical inductively coupled discharge configuration.

A. Electromagnetic model

The electromagnetic fields in the whole ICP reactor are governed by the Maxwell equations, which can be written as follows:

$$\nabla \times \mathbf{E} = -\frac{\partial \mathbf{B}}{\partial t}, \tag{1}$$

$$\nabla \times \mathbf{B} = \mu_0 \mathbf{J} + \varepsilon_0 \varepsilon_r \mu_0 \frac{\partial \mathbf{E}}{\partial t}, \tag{2}$$

where **E**, **B**, and **J** are the time-varying electric field, magnetic field, and the plasma current, respectively. ε_0, μ_0, and ε_r are the permittivity, the permeability of free space, and the relative dielectric constant of the dielectric window, respectively. The plasma current **J** equals zero in the vacuum vessel region and the dielectric window region. ε_r is set to 1 in the vacuum vessel region and plasma region.

In the present work, we assume that the discharge is in the purely inductive mode, in which the magnetic field is along the radial and axial directions and the electric field and plasma current only have an azimuthal component.

The boundary conditions are set as follows. The azimuthal electric field is set to zero at the wall of the metallic reactor, the bottom of the plasma region, and the top of the vacuum vessel. At the interface of two regions, the boundary relationships are set as follows. At the interface of plasma region and dielectric window

$$E_\theta(r,z)|_{z=h_1^-} = E_\theta(r,z)|_{z=h_1^+}, \tag{3}$$

$$B_r(r,z)|_{z=h_1^-} = B_r(r,z)|_{z=h_1^+}. \tag{4}$$

At the interface of dielectric window and vacuum vessel

$$\frac{1}{\mu_0}[B_r(r,z)|_{z=h_2^+} - B_r(r,z)|_{z=h_2^-}] = J_\theta(r), \tag{5}$$

$$E_\theta(r,z)|_{z=h_2^+} = E_\theta(r,z)|_{z=h_2^-}, \tag{6}$$

where $J_\theta(r)$ is the coil current distribution along the interface.

We solve the Maxwell equations using the finite difference time domain (FDTD) method to obtain the whole time and space information of the electromagnetic field. The Crank–Nicholson scheme is selected to solve the discrete Maxwell equations.

B. Fluid model

In the fluid model, the equations for electrons are as follows:

$$\frac{\partial n_e}{\partial t} + \nabla \cdot \mathbf{\Gamma}_e = R_e, \tag{7}$$

$$\frac{\partial}{\partial t}\left(\frac{3}{2} n_e k T_e\right) = -\nabla \cdot \mathbf{q}_e - e\mathbf{\Gamma}_e \cdot \mathbf{E} - E_e + P_{ind}. \tag{8}$$

Here, n_e denotes the electron density, $\mathbf{\Gamma}_e = n_e \mathbf{u}_e$ is the electron flux, $\mathbf{u}_e$ is the electron velocity, T_e is the electron temperature, k is the Boltzmann constant, and $\mathbf{E}$ is the static electric field. P_{ind} is the time-averaged power density deposited over one period and is expressed as $P_{ind} = 1/T \int_0^T J_\theta E_\theta dt$. $\mathbf{q}_e$ is the electron energy flux and can be described by the following equation:

$$\mathbf{q}_e = \frac{5}{2}\mathbf{\Gamma}_e k T_e - \frac{5}{2}\frac{n_e k T_e}{m_e \nu_{en}} \nabla (k T_e), \tag{9}$$

where ν_{en} is the collision frequency between electrons and neutral particles, m_e is the electron mass, and all other symbols have been explained above. R_e in Eq. (7) represents the electron generation rate due to electron impact ionization and can be written as

$$R_e = k_i(T_e) n_e n_a, \tag{10}$$

where k_i is the electron temperature dependent reaction rate coefficient of electron impact ionization of neutrals with density n_a. Our model is applied to an Ar ICP. The ionization rate coefficient for Ar is obtained from Ref. 31. E_e in Eq. (8) represents the total electron energy loss caused by various collisions of the electron with these neutrals

$$E_e = \sum_r \epsilon_r k_r(T_e) n_e n_a, \tag{11}$$

where ϵ_r is the average energy lost by the electrons per collision of type r and k_r is the reaction rate coefficient for different types of collisions. In our model, only ionization, total excitation, and momentum transfer with Ar atoms are taken into account. The rate coefficients for excitation and momentum transfer are also adopted from Ref. 31. The neutral Ar atom density n_a is assumed to be homogeneous and calculated through $P = n_a k T_a$, where P is the discharge pressure and T_a is the neutral gas temperature, which is set to be 300 K. The electron velocity $\mathbf{u}_e$ can be derived from the momentum equation

$$\frac{\partial \mathbf{u}_e}{\partial t} + (\mathbf{u}_e \cdot \nabla)\mathbf{u} = -\frac{e}{m_e}(\mathbf{E} + \mathbf{u}_e \times \mathbf{B}) - \frac{\nabla(n_e T_e)}{m_e n_e} - \nu_{en}\mathbf{u}_e, \tag{12}$$

where all symbols have been explained above. Both the inertia force and Lorentz force are considered in this equation. Below, we will show a comparison between the calculation results with and without taking the Lorentz force into account, in order to investigate its role in the harmonic effects.

In our model, all the physical quantities are calculated in the radial and axial directions, as we can assume azimuthal symmetry. Due to the acceleration of the azimuthal electron field E_θ, the azimuthal velocity u_θ is rather high. u_θ, E_θ, B_r, and B_z are therefore the fast variables with time. For simplification of the simulations, the inertia force term is neglected in Eq. (12) above and the drift-diffusion approximation is used for the radial and axial components. Accordingly, the three components of the momentum equation can be written as follows:

$$u_r = -\frac{e}{m_e \nu_e}(E_r + u_\theta B_z) - \frac{1}{m_e n_e \nu_e}\frac{\partial}{\partial r}(n_e T_e), \tag{13}$$

$$u_z = -\frac{e}{m_e \nu_e}(E_z + u_\theta B_r) - \frac{1}{m_e n_e \nu_e}\frac{\partial}{\partial z}(n_e T_e), \tag{14}$$

$$\frac{\partial u_\theta}{\partial t} + u_r\frac{\partial u_\theta}{\partial r} + u_z\frac{\partial u_\theta}{\partial z} + \frac{u_r u_\theta}{r} = -\frac{e}{m_e}(E_\theta + u_z B_r - u_r B_z) - \nu_e u_\theta. \tag{15}$$

j_θ can be calculated from u_θ as $-e n_e u_\theta$.

The behavior of the ions is governed by the continuity and momentum equation

$$\frac{\partial n_i}{\partial t} + \nabla \cdot n_i \mathbf{u}_i = R_i, \tag{16}$$

$$\frac{\partial n_i m_i \mathbf{u}_i}{\partial t} + \nabla \cdot (n_i m_i \mathbf{u}_i \mathbf{u}_i) = -kT_i \nabla n_i + e n_i \mathbf{E} - \mathbf{M}_i, \tag{17}$$

where n_i is the ion density, $\mathbf{u}_i$ is the ion velocity, m_i is the ion mass, and T_i is the ion temperature. R_i represents the ion generation due to electron ionization collisions and it is equal to R_e in Eq. (6). $\mathbf{M}_i$ represents the collisional transfer of momentum from ions to neutral species.

The Poisson equation is solved to obtain the static electric field $\mathbf{E}$ caused by the plasma space charge

$$\nabla^2 \phi(r,z) = -\frac{e}{\varepsilon_0}(n_i - n_e), \tag{18}$$

where ϕ is the potential and ε_0 is the permittivity of free space.

The boundary conditions and the specific method to solve the above equations are described in detail in Ref. 6.

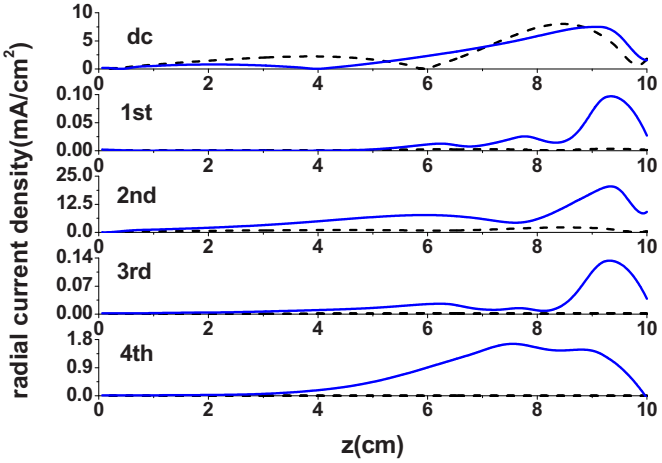

FIG. 2. (Color online) Comparison of the different harmonic components of the radial current density along the *z*-direction, calculated from the model without Lorentz force (dashed line) and with Lorentz force (solid line) at 10 mTorr and 3.39 MHz.

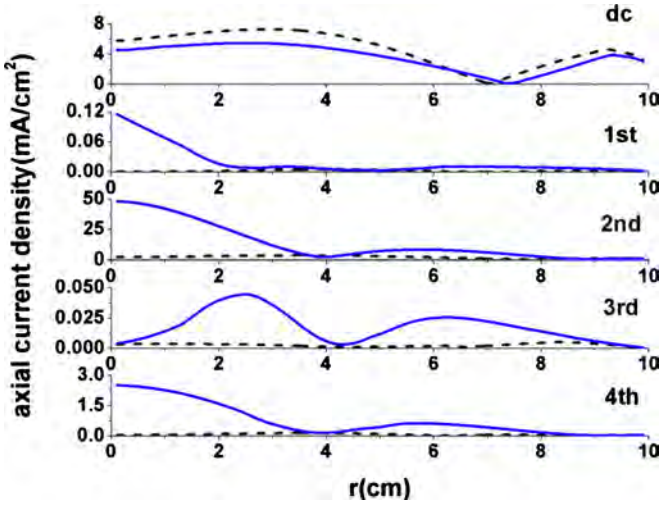

FIG. 3. (Color online) Comparison of the different harmonic components of the axial current density along the *r*-direction, calculated from the model without Lorentz force (dashed line) and with Lorentz force (solid line) at 10 mTorr and 3.39 MHz.

III. RESULTS AND DISCUSSIONS

In this section, different harmonic components of the current density, calculated with and without nonlinear Lorentz force, are compared at fixed driving frequency, in order to investigate the role of the Lorentz force on the harmonic effects. Furthermore, the direct current (dc) and second and fourth harmonic components of the radial and axial current density, as well as the harmonic components of the potential at different frequencies, are also presented in order to illustrate the harmonic effects on current density and potential since it is found in the literature that plasma nonlinear polarization plays an important role in affecting these parameters at lower frequency. Finally, since the current density and potential will influence the plasma behavior, some important plasma quantities, such as the deposited power density, plasma density, plasma temperature, and azimuthal electric field, are also illustrated for different frequencies to investigate the impact of the harmonic effects on these plasma quantities. The Ar gas pressure is fixed at 10 mTorr and the frequencies are set as 3.39, 6.78, and 13.56 MHz, respectively. The deposited power is fixed at 133 W.

All the plasma quantities in our simulation are expanded as follows:

$$\Psi(\mathbf{r},t) = \Psi_0(\mathbf{r}) + \sum_{n=1}^{\infty} \Psi_n(\mathbf{r}) e^{i(n\omega t+\phi_n)}, \tag{19}$$

where $\Psi(\mathbf{r},t)$ represents different plasma quantities simulated in this paper, such as the current density, plasma potential, and the electromagnetic field. $\Psi_n(\mathbf{r})(n=0,1,2,\ldots)$ and ϕ_n are the amplitude and phase of the different harmonic components.

A. Comparison of harmonic components with and without nonlinear Lorentz force

Figure 2 shows the different harmonic components of the radial harmonic current density as a function of axial position in the reactor, calculated with and without Lorentz force at 3.39 MHz at $r=4.9$ cm. In the case without Lorentz force (see dashed lines), the dc component of the radial current density is clearly dominant and the other components are rather weak. Indeed, the current density is virtually resonant linearly when calculated without nonlinear Lorentz force. It appears that the amplitude and spatial profile of the dc component are hardly influenced by the Lorentz force. However, when the Lorentz force is taken into account, the second harmonic component clearly dominates. Besides, the dc, second, and fourth harmonic components are much larger than the first and third harmonic components in this case.

These effects can be explained using the expansion of the electron equation of motion, described in the Appendix. The dc component of the current density is composed by the diffusion term and a term related to the nonlinear Lorentz force, shown in Eq. (A13). For an ICP, when the power is not too high and the driving frequency is not too low, the diffusion term is larger than the other term. Thus, the dc component remains almost the same whether the nonlinear Lorentz force is taken into account or not. Furthermore, the ratio of the second harmonic component to the first harmonic component of current density is shown in Eq. (A14). We can find out that the ratio is much larger than 1, when the electric field is strong and the driving frequency is low. The third and fourth harmonic components could also be derived using the same method described in the Appendix.

The comparison of the different harmonic components of the axial harmonic current density, calculated with and without Lorentz force, is illustrated in Fig. 3 as a function of radial position and $z=3.3$ cm at 3.39 MHz. Again, the dc component is the dominant one in the case without Lorentz force because of the assumption of harmonic approximation. Also, the dc component looks quite similar (both in absolute value and the spatial dependence) with and without Lorentz force. Moreover, the second harmonic is again the largest

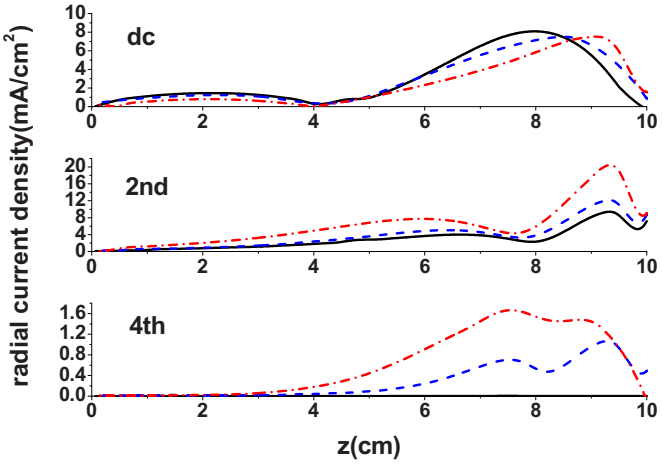

FIG. 4. (Color online) Comparison of the dc, second, and fourth harmonic components of the radial current density along the z-direction at 13.56 (solid line), 6.78 (dashed line), and 3.39 MHz (dotted line).

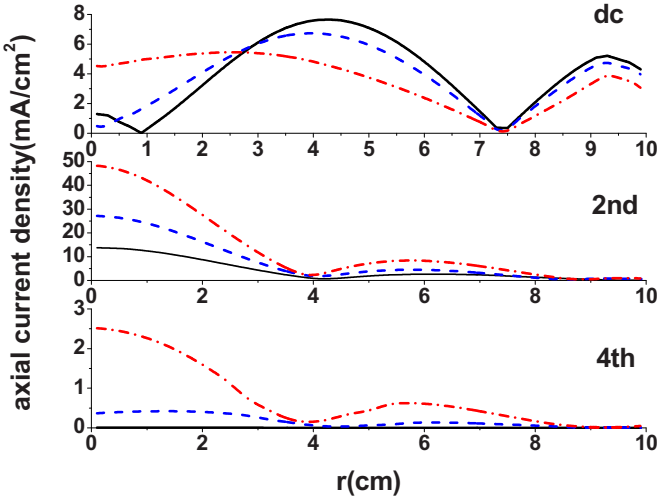

FIG. 5. (Color online) Comparison of the dc, second, and fourth harmonic components of the axial current density along the *r*-direction at 13.56 (solid line), 6.78 (dashed line), and 3.39 MHz (dotted line).

component if the Lorentz force is taken into account and the first and third harmonic can again be neglected, for the same reasons as explained above.

From the above analysis, we can see that the nonlinear term in Eq. (12), i.e., the Lorentz force, significantly affects the formation of harmonic currents, especially the even harmonic components. This means that the Lorentz force should certainly be included in fluid models of an ICP operating at low frequency.

In the following, we will display only the dc, second, and fourth harmonic components, since the other components are so small that they can be ignored.

B. Harmonic current density components at different frequencies

Since the nonlinear plasma polarization will obviously influence the current density, especially at lower frequency, a comparison among the dc, second, and fourth harmonic components of the radial current density at different driving frequencies is illustrated in Fig. 4 as a function of axial position, at $r=4.9$ cm, in order to elucidate this phenomenon. The amplitude of the dc radial current density remains almost the same when lowering the driving frequency. Meanwhile, the amplitude of the second and fourth harmonics of the current density increase with decreasing frequency, since the nonlinear Lorentz force becomes larger at lower frequency. Note that the fourth harmonic component at the largest frequency investigated, i.e., 13.56 MHz, is even negligible. The second harmonic component reaches its maximum at about $z=9.2$ cm at the three frequencies investigated and is transferred along the axial direction by electron thermal motion. The peak of the electron density at the symmetry axis will enhance the current density there and the maximal radial current density appears near the symmetry axis. The positions of the second maximum of the second harmonic and the peak of the fourth harmonic shift slightly away from the symmetry axis with decreasing frequency due to the phase influence of these components.

Figure 5 illustrates the different harmonic components of the axial current density at different frequencies as a function of radial position at $z=3.3$ cm. The amplitude of the dc axial current density slightly drops with decreasing frequency. The second and fourth harmonics of the axial current density are clearly higher at lower driving frequency, but the positions of the minima of the two harmonic components are almost unchanged and fixed at $r=4.0$ cm. It is consistent with the position where the phase of the second harmonic component changes abruptly. The position of the maximum of the second harmonic component is at the symmetry axis since the highest plasma density will enhance the current density at the axis. Besides, the fourth harmonic at 13.56 MHz is again too small to be detected.

The rise in the harmonic components with decreasing frequency indicates that the nonlinear effects become more obvious at low frequency, which can be attributed to the nonlinear Lorentz force. Indeed, according to the Maxwell equation, we can obtain the relationship $E \propto \omega B$. Thus, the rf magnetic field $B \propto \omega^{-1}$ is larger at lower frequency and, therefore, the Lorentz force, which is the origin of the harmonic effects, becomes more important at lower frequency. The trend of the simulation results is consistent with experimental results,[21] although the specific values are different because of the different operating conditions.

C. Harmonic potential

The plasma potential is an important ICP characteristic which will influence the performance of ICP sources. Figure 6 shows each harmonic component of the potential at 3.39 MHz at the positions $z=2.0625$ cm and $r=4.9$ cm. The dc component is still the largest one among the harmonic components. The second harmonic will dominate in the other harmonics and, in general, the even harmonic components are again much larger than the adjacent odd harmonic components. The origin of the second and higher harmonics is again due to the nonlinear effect caused by the Lorentz force. This quadratic effect $[B_{\mathrm{rf}} v_{\mathrm{rf}} \propto B_{\mathrm{rf}}^2 \propto \sin^2(\omega t)]$ is more signifi-

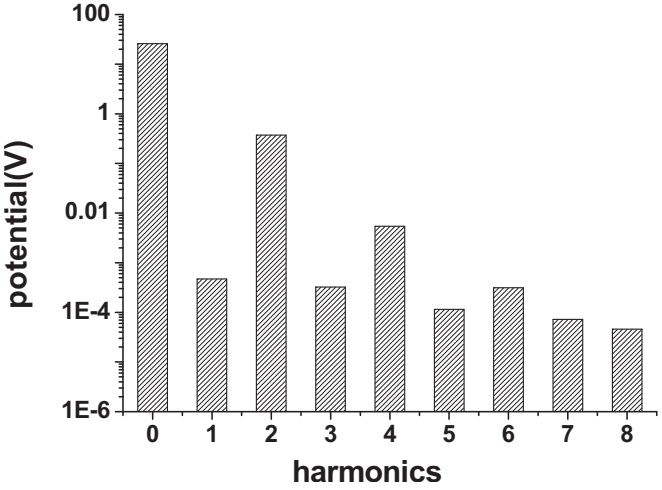

FIG. 6. The spectrum of harmonic components of the potential at $z=2.0624$ cm and $r=4.9$ cm at 10 mTorr and 3.39 MHz.

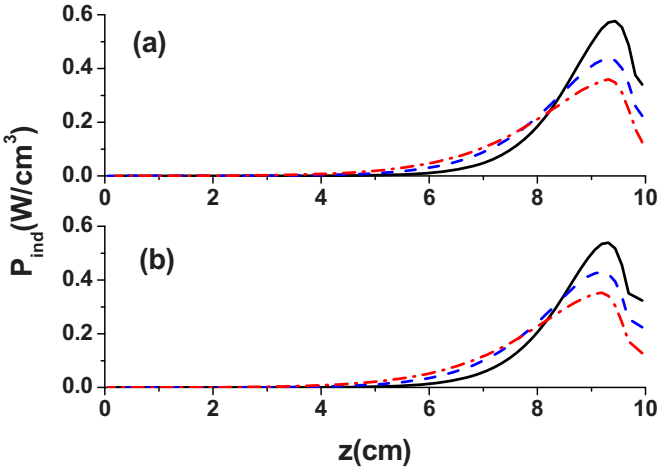

FIG. 8. (Color online) Comparison of the deposited rf power density along the z-direction at 13.56 (solid line), 6.78 (dashed line), and 3.39 MHz (dotted line). (a) Model without the Lorentz force; (b) model with the Lorentz force.

cant at low pressure and low frequency when both the electron drift velocity and magnetic field are large. We will only discuss the second harmonic potential below since it is the dominant one in the higher harmonics.

Figure 7 illustrates the second harmonic component of the potential along the axial direction at a radial position of 4.9 cm at different driving frequencies. Similar to the current density behavior, the second harmonic potential, which drops sharply in the skin layer, increases with decreasing frequency since the nonlinear Lorentz force becomes larger at lower driving frequency. This trend is consistent with the nonlinear polarization field. Our simulation results are also consistent with the experimental results presented by Godyak *et al.*[25] However, the absolute value calculated is ten times smaller than the experimental data and the dc component is larger than the second component in our simulation, while the two components are comparable in the experiment. This is attributed to the higher power, lower pressure, and lower frequency applied in the experiments, which could not be used in our model due to the limitation of stabilization at such conditions.

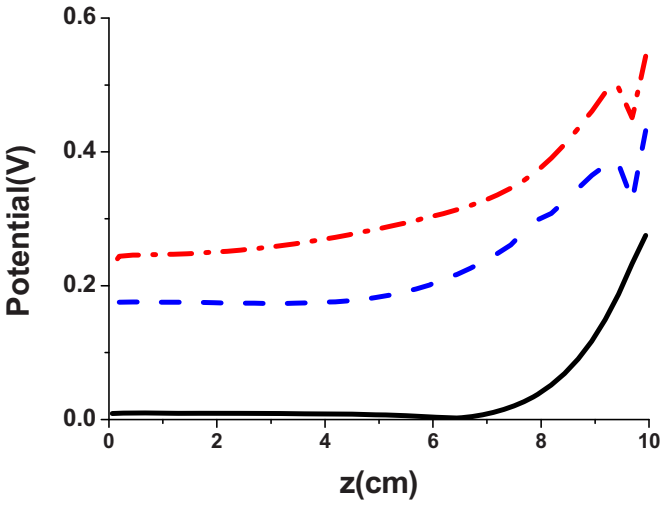

FIG. 7. (Color online) Second harmonic component of the potential as a function of axial position at a radial position of 4.9 cm at 10 mTorr at 13.56 (solid line), 6.78 (dashed line), and 3.39 MHz (dotted line).

D. Deposited power density, plasma density, electron temperature, and azimuthal electric field

Figure 8 shows the comparison between the deposited rf power density P_{ind} as a function of axial position in the reactor, calculated with and without Lorentz force at different driving frequencies at $r=4.9$ cm. We should note that the total deposited power is fixed at 133 W in our calculation. The maximum of the deposited rf power decreases and the depth of the skin layer increases slightly when the nonlinear Lorentz force is taken into account, since the ponderomotive force, induced by the nonlinear Lorentz force, drives the electron to transit more deeply into the plasma. Furthermore, it is observed from both Figs. 8(a) and 8(b) that the maximum of the deposited power density decreases for lower frequency, whether the nonlinear Lorentz force is taken into account or not.

The comparison of the plasma density at different frequencies, calculated with and without Lorentz force, is illustrated in Fig. 9 as a function of axial position at $r=4.9$ cm. The plasma density decreases slightly with decreasing frequency and a maximum in the axial direction is reached at about 3 cm from the top of the plasma region, both with and without the nonlinear Lorentz force. Comparison between Figs. 9(a) and 9(b) shows that the plasma density calculated with the Lorentz force is higher than the results without the Lorentz force, since the higher harmonic current density acts on the plasma when the Lorentz force is taken into account.

The electron temperature profile, calculated with and without Lorentz force, as a function of axial position is plotted in Fig. 10, again at the three different frequencies at $r=4.9$ cm. The maximum of electron temperature is on the top of the plasma region, just beneath the coil, i.e., where the electrons gain most energy from the electromagnetic field. The electron temperature remains almost the same when cal-

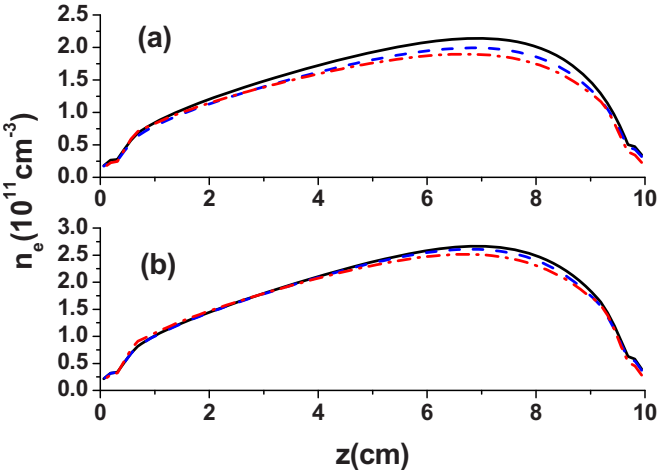

FIG. 9. (Color online) Comparison of the plasma density along the *z*-direction at 13.56 MHz (solid line), 6.78 (dashed line), and 3.39 MHz (dotted line). (a) Model without the Lorentz force; (b) model with the Lorentz force.

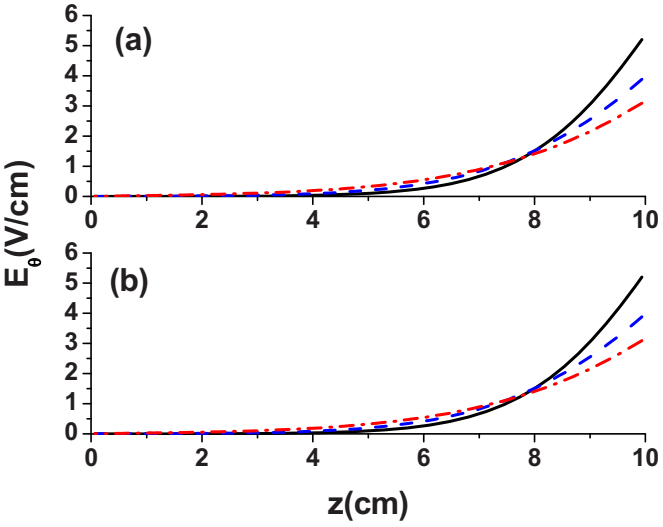

FIG. 11. (Color online) Comparison of the azimuthal electric field along the *z*-direction at 13.56 (solid line), 6.78 (dashed line), and 3.39 MHz (dotted line). (a) Model without the Lorentz force; (b) model with the Lorentz force.

culated with and without the Lorentz force, since the diffusion process in the steady plasma eliminates the effects of the nonlinear Lorentz force to a certain extent. The electron temperature drops at lower frequency, especially in the skin layer, which is correlated with the somewhat lower deposited power density at lower frequency.

Figure 11 shows the azimuthal electric field as a function of axial position in the reactor, calculated with and without Lorentz force at different frequencies at $r=4.9$ cm at the beginning of the rf period. The maximum of the azimuthal electric field decreases and the depth of the skin layer increases slightly when the nonlinear Lorentz force is taken into account. Moreover, the maximum of the azimuthal electric field decreases with decreasing frequency, whether the nonlinear Lorentz force is taken into account or not.

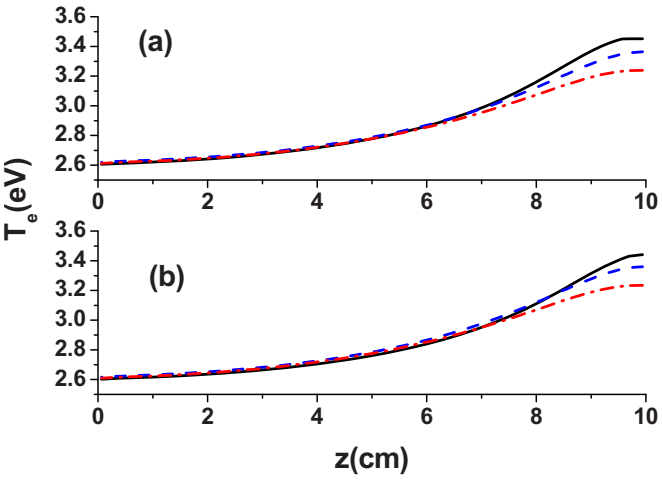

FIG. 10. (Color online) Comparison of the electron temperature along the *z*-direction at 13.56 (solid line), 6.78 (dashed line), and 3.39 MHz (dotted line). (a) Model without the Lorentz force; (b) model with the Lorentz force.

IV. CONCLUSIONS

In this work, we have developed a self-consistent model, based on an electromagnetic model and a fluid model, to simulate the harmonic effects in an ICP. The electromagnetic field is solved using the FDTD technique to obtain the whole information of time and space instead of using the harmonic assumption in solving the Maxwell equations. The obvious differences between the model with and without nonlinear Lorentz force have been illustrated by comparing all the harmonic components of the radial and axial current densities. The even harmonic components are usually larger than the odd ones and the second harmonic always dominates when the nonlinear force is taken into account. Our simulation has proved that the nonlinear Lorentz force is exactly the origin of the second harmonic current density.

As illustrated in the comparison of the different harmonic components of the axial and radial current density at different frequencies, the harmonic effects become significant at lower frequency. The amplitude of the dc component appears almost the same at different frequencies, while the second and fourth harmonic components of the current density increase with decreasing frequency, since the nonlinear Lorentz force is stronger at lower frequency.

We have also investigated the harmonic components of the potential at different driving frequencies. The harmonic components of the potential also increase with decreasing frequency which is also related to the nonlinear Lorentz force. Besides, the even harmonics are larger than the next odd harmonics which is consistent with the experiment, although the absolute values are smaller in our simulation.

The deposited power density, electron density, electron temperature, and azimuthal electric field calculated with and without the nonlinear Lorentz force are also investigated in this work. The peak of the deposited power density decreases and the depth of the skin layer increases slightly when the Lorentz force is taken into account, since the electron penetrates more deeply into the plasma under the action of the

Lorentz force. Moreover, the plasma density increases since the harmonic current density is higher when the Lorentz force is included. The deposited power density increases and the depth of penetration decreases with increasing frequency because of the frequent collisions at high driving frequency at a constant total deposited power. The electron density and electron temperature also decrease with decreasing frequency, which is consistent with the trend of the deposited power density. The azimuthal electric field decreases slightly with decreasing frequency and the depth of penetration increases when the Lorentz force is taken into account. Indeed, the nonlinear Lorentz force, which influences the current density and plasma potential, also affects in this way the other plasma quantities, such as the deposited power density and the electron density.

ACKNOWLEDGMENTS

This work was supported by the National Natural Science Foundation of China (Grant No. 11075029), the Specialized Research Fund for the Doctoral Program of Higher Education (Grant No. 20090041110026), and the joint research project in the framework of the agreement between MOST and FWO.

APPENDIX: SECOND-ORDER PERTURBED EXPANSION OF THE ELECTRON EQUATION OF MOTION

When the nonlinear convection term in the left-hand side of Eq. (12) is neglected, the electron momentum equation can be written as

$$\frac{\partial \mathbf{u}_e}{\partial t} = -\frac{e}{m_e}(\mathbf{E} + \mathbf{u}_e \times \mathbf{B}) - \frac{\nabla(n_e T_e)}{m_e n_e} - \nu_{en}\mathbf{u}_e. \tag{A1}$$

In the following discussions, we can assume that $\mathbf{E}(\mathbf{r},t) = \mathbf{E_0}(\mathbf{r})\cos(\omega t)$ and the electron density and electron temperature do not vary significantly with time, i.e., zero-order perturbed quantities, since they are the slow variables with time. Following Chen's derivation,[32] we can write

$$\mathbf{u}_e = \mathbf{u_0} + \mathbf{u_1} + \mathbf{u_2} + \cdots, \tag{A2}$$

$$\mathbf{E}(\mathbf{r},t) = [\mathbf{E_0}(\mathbf{r_0}) + (\delta\mathbf{r_1}\cdot\nabla)\mathbf{E_0}(\mathbf{r_0}) + \cdots]\cos(\omega t), \tag{A3}$$

where $\mathbf{r_0}$ is the electron initial position and $\delta\mathbf{r_1}$ is the change in electron position with time. In the weakly collisional case where $\nu_{en} \ll \omega$, we substitute Eqs. (A2) and (A3) into Eq. (A1) and can find

$$\mathbf{u_0} = -\frac{1}{m_e n_e \nu_{en}}\nabla(n_e T_e), \tag{A4}$$

$$\mathbf{u_1} = -\frac{e}{m_e\omega}\mathbf{E_0}\sin(\omega t), \tag{A5}$$

$$\mathbf{u_2} = \frac{1}{m_e\nu_{en}}\mathbf{F_{dc}} + \frac{\mathbf{F_{2\omega}}}{2m_e\omega}\sin(2\omega t), \tag{A6}$$

where $\mathbf{F_{dc}}$ and $\mathbf{F_{2\omega}}$ are the dc part and the second-order nonlinear force, respectively, and can be expressed as

$$\mathbf{F_{dc}} = -\frac{e^2}{4m_e\omega^2}\nabla E_0^2, \tag{A7}$$

$$\mathbf{F_{2\omega}} = \frac{e^2}{m_e\omega^2}\left[(\mathbf{E_0}\cdot\nabla)\mathbf{E_0} - \frac{\nabla E_0^2}{4}\right]. \tag{A8}$$

The current density $\mathbf{j}$ can be written as

$$\mathbf{j} = \mathbf{j_{dc}} + \mathbf{j_1}\sin(\omega t) + \mathbf{j_2}\sin(2\omega t), \tag{A9}$$

where $\mathbf{j_{dc}}$, $\mathbf{j_1}$, and $\mathbf{j_2}$ are the zero, first, and second harmonic components of the current density and can be expressed as follows:

$$\mathbf{j_{dc}} = \frac{e}{m_e\nu_{en}}\nabla(n_e T_e) + \frac{e^3 n_e}{4\nu_{en}m_e^2\omega^2}\nabla E_0^2, \tag{A10}$$

$$\mathbf{j_1} = \frac{e^2 n_e}{m_e\omega}\mathbf{E_0}, \tag{A11}$$

$$\mathbf{j_2} = -\frac{e^3 n_e}{2m_e^2\omega^3}\left[(\mathbf{E_0}\cdot\nabla)\mathbf{E_0} - \frac{\nabla E_0^2}{4}\right]. \tag{A12}$$

The dc component of the current density can be estimated as

$$j_{\mathrm{dc}} \approx \frac{n_e e}{m_e\nu_{en}L}\left[T_e + \frac{e^2}{4m_e\omega^2}E_0^2\right], \tag{A13}$$

where L is the dimension of the plasma chamber. The first term is the diffusion term and the second term is induced by the nonlinear Lorentz force. The second term is larger than the diffusion term, when the frequency is low enough and the power P_{rf} is high enough, since $P_{\mathrm{rf}} \propto E_0^2$.

The absolute value of the ratio j_2/j_1 can be estimated as

$$\left|\frac{j_2}{j_1}\right| \approx \frac{eE_0}{8m_e\omega^2 L}. \tag{A14}$$

Of course, the ratio is much larger than 1 in the condition that the electric field is strong and the driving frequency is low.

[1] M. A. Lieberman and A. J. Lichtenberg, *Principles of Plasma Discharges and Materials Processing*, 2nd ed. (Wiley-Interscience, New York, 2005).
[2] M. Avella, J. Jimnez, F. Pommereau, J. P. Landesman, and A. Rhallabi, Appl. Phys. Lett. **93**, 131913 (2008).
[3] A. Efremov, N. K. Min, J. Jeong, Y. Kim, and K. Kwon, Plasma Sources Sci. Technol. **19**, 045020 (2010).
[4] J. S. Li, J. X. Wang, M. Yin, P. Q. Gao, D. Y. He, Q. Chen, Y. L. Li, and H. Shirai, J. Appl. Phys. **103**, 043505 (2008).
[5] I. B. Denysenko, S. Xu, J. D. Long, P. P. Rutkevych, N. A. Azarenkov, and K. Ostrikov, J. Appl. Phys. **95**, 2713 (2004).
[6] F. Gao, S. X. Zhao, X. S. Li, and Y. N. Wang, Phys. Plasmas **16**, 113502 (2009).
[7] H. Fukumoto, I. Fujikake, Y. Takao, K. Eriguchi, and K. Ono, Plasma Sources Sci. Technol. **18**, 045027 (2009).
[8] H. C. Lee, M. H. Lee, and C. W. Chung, Phys. Plasmas **17**, 013501 (2010).
[9] T. Kimura and H. Kasugai, J. Appl. Phys. **107**, 083308 (2010).
[10] J. Hopwood, Plasma Sources Sci. Technol. **1**, 109 (1992).
[11] I. M. El-Fayoumi and I. R. Jones, Plasma Sources Sci. Technol. **7**, 162 (1998).
[12] K. N. Ostrikov, K. B. Denysenko, E. L. Tsakadze, S. Xu, and R. G. Storer, J. Appl. Phys. **92**, 4935 (2002).
[13] G. Cunge, B. Crowley, D. Vender, and M. M. Turner, J. Appl. Phys. **89**, 3580 (2001).

[14]Y. O. Tyshetskiy, A. I. Smolyakov, and V. A. Godyak, Phys. Rev. Lett. **90**, 255002 (2003).
[15]I. D. Kaganovich, O. V. Polomarov, and C. E. Theodosiou, Phys. Plasmas **11**, 2399 (2004).
[16]Y. O. Tyshetskiy, A. I. Smolyakov, and V. A. Godyak, Plasma Sources Sci. Technol. **11**, 203 (2002).
[17]G. J. M. Hagelaar, Plasma Sources Sci. Technol. **17**, 025017 (2008).
[18]S. Xu, K. N. Ostrikov, W. Luo, and S. Lee, J. Vac. Sci. Technol. A **18**, 2185 (2000).
[19]A. M. Daltrini, S. A. Moshkalev, M. J. R. Monteiro, E. Besseler, A. Kostryukov, and M. Machida, J. Appl. Phys. **101**, 073309 (2007).
[20]S. X. Zhao, X. Xu, X. C. Li, and Y. N. Wang, J. Appl. Phys. **105**, 083306 (2009).
[21]V. A. Godyak, R. B. Piejak, and B. M. Alexandrovich, Phys. Rev. Lett. **83**, 1610 (1999).
[22]R. H. Cohen and T. D. Rognlien, Phys. Plasmas **3**, 1839 (1996).
[23]V. A. Godyak, R. B. Piejak, and B. M. Alexandrovich, J. Appl. Phys. **85**, 703 (1999).
[24]V. A. Godyak, R. B. Piejak, B. M. Alexandrovich, and V. I. Kolobov, Phys. Plasmas **6**, 1804 (1999).
[25]V. A. Godyak, B. M. Alexandrovich, R. B. Piejak, and A. I. Smolyakov, Plasma Sources Sci. Technol. **9**, 541 (2000).
[26]A. Smolyakov, V. Godyak, and A. Duffy, Phys. Plasmas **7**, 4755 (2000).
[27]R. B. Piejak and V. A. Godyak, Appl. Phys. Lett. **76**, 2188 (2000).
[28]K. Ostrikov, E. Tsakadze, S. Xu, S. V. Vladimirov, and R. Storer, Phys. Plasmas **10**, 1146 (2003).
[29]A. V. Vasenkov and M. J. Kushner, J. Appl. Phys. **94**, 2223 (2003).
[30]A. I. Smolyakov, V. A. Godyak, and Y. O. Tyshetskiy, Phys. Plasmas **10**, 2108 (2003).
[31]J. D. Bukowski, D. B. Graves, and P. Vitello, J. Appl. Phys. **80**, 2614 (1996).
[32]F. F. Chen, *Introduction to Plasma Physics* (Plenum, New York, 1974), p. 256.